A Tutorial: Adaptive Runge-Kutta Integration for Stiff Systems: Comparing the Nosé and Nosé-Hoover Oscillator Dynamics

William Graham Hoover and Julien Clinton Sprott and Carol Griswold Hoover

Ruby Valley Research Institute and Department of Physics University of Wisconsin-Madison

Corresponding Author email : hooverwilliam@yahoo.com

Madison, Wisconsin 53706

Highway Contract 60, Box 601, Ruby Valley, Nevada 89833, USA ;

(Dated: September 26, 2016)

Abstract

"Stiff" differential equations are commonplace in engineering and dynamical systems. To solve them we need flexible integrators that can deal with rapidly-changing righthand sides. This tutorial describes the application of "adaptive" [variable timestep] integrators to "stiff" mechanical problems encountered in modern applications of Gibbs' 1902 statistical mechanics. Linear harmonic oscillators subject to *nonlinear* thermal constraints can exhibit either stiff or smooth dynamics. Two closely-related examples, Nosé's 1984 dynamics and Nosé-Hoover 1985 dynamics, are both based on Hamiltonian mechanics, as was ultimately clarified by Dettmann and Morriss in 1996. Both these dynamics are consistent with Gibbs' canonical ensemble. Nosé's dynamics is "stiff" and can present severe numerical difficulties. Nosé-Hoover dynamics, though it follows *exactly the same* trajectory, is "smooth" and relatively trouble-free. Our tutorial emphasises the power of *adaptive* integrators to resolve stiff problems like the Nosé oscillator. The solutions obtained illustrate the power of computer graphics to enrich numerical solutions. Adaptive integration with computer graphics is basic to an understanding of dynamical systems and statistical mechanics. These tools lead naturally into the visualization of intricate fractal structures formed by chaos as well as elaborate knots tied by regular nonchaotic dynamics. This work was invited by the American Journal of Physics.

I. INTRODUCTION AND OVERVIEW

Nosé's very original 1984 work extended classical *isoenergetic* Newtonian molecular dynamics to include a new temperature-based dynamics. His goal was to replicate Gibbs' *isothermal* canonical ensemble directly from dynamics. Nosé based his work on isoenergetic Hamiltonian mechanics[1–6]. The resulting motion equations are typically "stiff" and hard to solve. Nosé introduced the idea of "time-scaling" to cope with these difficulties. Hoover pointed out that a smoothed and improved set of motion equations could be based on Liouville's Theorem without the need for time-scaling or a Hamiltonian basis[4]. Dettmann furnished a Hamiltonian basis linking both sets of motion equations a decade later in 1996[5,6].

Both the original Nosé dynamics and the improved Nosé-Hoover dynamics share a common flaw. They are not necessarily "ergodic". Their phase-space flows cover only a fraction of the available states, even for the simplest (harmonic-oscillator) applications[5–10]. It was not until 2015 that an ergodic analog of Nosé's dynamics was discovered[9], reaching a goal of his original 1984 project.

Nosé's work provides many opportunities for further study and improvements. We include here side-by-side calculations for the (stiff) Nosé and (smooth) Nosé-Hoover oscillators. These two oscillator types follow *exactly the same* phase-space trajectory but at different rates. The dynamics for these oscillators are related to each other by "time scaling". In fact, the *four*-dimensional descriptions of the two models' detailed trajectories are precisely identical ! But of the two only Nosé's oscillator problem exhibits the stiffness which is the focus of the present work.

The Nosé oscillator was designed to model a harmonic oscillator at thermal equilibrium, characterized by a temperature T. The dynamics Nosé developed has both regular [stable to small perturbations] and chaotic [unstable to perturbations] solutions, coexisting in a constant-energy three-dimensional volume within a four-dimensional phase space. Within that space there are infinitely-many regular solutions (concentric tori and stable periodic orbits) in addition to a single chaotic sea which stretches to infinity and occupies about six percent of the stationary measure defined by Liouville's Theorem. Quite remarkably that stationary measure has a simple analytic form. It is a smooth three-dimensional Gaussian distribution. Though the simpler regular stable tori and the periodic orbits they enclose are relatively easy to solve, motion in Nosé's version of the chaotic sea is sufficiently stiff to

require the special solution methods we describe in what follows.

Typical fixed-timestep integrators like leapfrog and fourth-order Runge-Kutta are ineffective in Nosé's chaotic sea. We emphasize here a family of useful alternatives, simple variable-timestep "adaptive" algorithms[11]. We explore Nosé's work with their aid. *Adaptive* techniques vary the numerical algorithms' timestep to compensate for time-dependent changes in the stiffness of the underlying ordinary differential equations. The present Tutorial is intended to introduce students and researchers to both the Nosé and Nosé-Hoover oscillator example problems and to their solution using adaptive integration. We connect "stiffness" with time-stepping, time-scaling, and Lyapunov instability. In exploring these numerical features of our models we come upon intricate topologies with their roots in simple quadratic differential equations.

We recommend the Nosé oscillator to students as a testbed for integrators, computer graphics, and numerical methods. This picturesque model provides challenges in visualizing the fascinating topology of knots and island chains in readily accessible three- and four-dimensional phase spaces. The model's simple structure makes it an ideal introduction to dynamical-systems research.

In Section II we detail the statistical-mechanical background which links the Nosé and Nosé-Hoover models. In Section III we introduce a family of flexible integrators capable of accurate solutions of the stiff oscillator problems. In Section IV we choose and apply a common initial condition for our dynamic investigations of time-scaling and stiffness. This choice makes our work reproducible. We illustrate the evolution of Nosé's time-scaling factor "s", the adaptive timestep dt, and the local Lyapunov exponent, $\lambda_1(t)$. We compare simulations with both double- and quadruple-precision arithmetic, 64 and 128 binary bits respectively. In Section V we take stock of what we have learned and suggest areas for further investigations using our new tools.

II.   NOSÉ AND NOSÉ-HOOVER DYNAMICS FOR HARMONIC OSCILLATORS

In 1984 Shuichi Nosé imagined a temperature-dependent Hamiltonian $\mathcal{H}_N$ with a "time-scaling" control variable $0 < s < 1$. This "invention", or better yet, "discovery", provides a unique s-dependent dynamics. The speed at which a thermal trajectory evolves is governed by s , which in turn controls the kinetic temperature T. The dynamics is consistent (in the
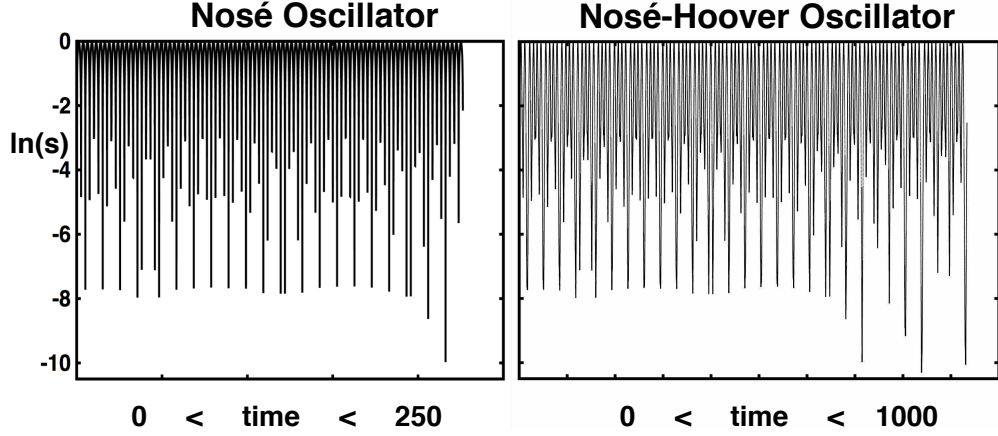
FIG. 1: The variation of the [Nosé] (at the left) and [Nosé-Hoover #1] (at the right) time-scaling factors s with time. See subsection IIA of the text for the differential equations solved here. In principle exactly the same values of (q, p, s, ζ) and, in the same order, apply to both models. Both models were solved for 100 000 adaptive-integrator timesteps. The adaptive RK4 timestep is doubled whenever the rms discrepancy between a single dt timestep and two $(dt/2)$ half timesteps is less than 10^{-12} . The timestep is halved if the discrepancy is greater than 10^{-10} . The minimum value of s within this fragment is about $e^{-10} \simeq 0.00005$. The initial conditions for both these simulations are $(q, p, s, \zeta, \mathcal{H}) = (2.4, 0, e^{-2.88}, 0, 0)$, chosen so that the Hamiltonian $\mathcal{H}$ vanishes. All four Nosé-Hoover rates are smaller than the Nosé rates by a factor of $s(t)$.

"necessary but insufficient" sense) with Gibbs' canonical ensembles of constant-temperature states rather than the more usual "microcanonical" ensembles of constant-energy states. In conventional oscillator mechanics the total energy $\mathcal{H} = (1/2)(q^2 + p^2)$ is constant where q and p are the oscillator displacement and momentum. That usual oscillator dynamics generates sine and cosine solutions with vibrational amplitudes proportional to the square

root of the kinetic temperature p^2 .

$$\langle\, q^2\,\rangle = \langle\, p^2\,\rangle = T = \langle\,\mathcal{H}\,\rangle\ .$$

In Nosé's s-dependent mechanics temperature is likewise a measure of the kinetic energy, $T \propto (p/s)^2$, where (p/s) is a *scaled* Cartesian momentum component. In the simplest harmonic-oscillator case Nosé's approach uses s to *scale* the momentum over a broad range. The scale factor s varies from its maximum, unity, to less than 10^{-9} over a billion-timestep adaptive simulation where the mean timestep is about 0.002. See the shorter 100 000-timestep oscillator histories shown in **Figure 1**. We detail a useful approach to such problems in what follows.

Throughout this Tutorial we adopt the simplest possible notation so as to focus on the basic ideas. We choose to explore the behavior of a harmonic oscillator with unit mass and force constant. In keeping with simplicity (and without loss of generality) we also set Boltzmann's constant and the temperature equal to unity.

Nosé's *time-scaled* Hamiltonian (where s is the time-scaling factor and ζ is its conjugate momentum) for the isothermal one-dimensional harmonic oscillator is :

$$2\mathcal{H}_N = q^2 + (p/s)^2 + \ln(s^2) + \zeta^2 \equiv 0 \ [\ \text{Nosé}\ ]\ .$$

Here and in what follows we consistently choose the soon-to-be-explained significant value of the Hamiltonian $\mathcal{H}_N \equiv 0$. This Hamiltonian governs the evolution of the four time-dependent variables (q, p, s, ζ) . q and p are still the usual oscillator coordinate and momentum, though with the usual link between velocity and momentum changed. The Cartesian relation $\dot{q} = p$ is replaced by $\dot{q} = (\partial\mathcal{H}_N/\partial p) = (p/s^2)$. Because the canonical distribution includes states with *all* energies, $0 < \mathcal{H} < \infty$, Nosé had the idea to include the "time-scale factor" s, along with its conjugate momentum ζ, *in* the Hamiltonian, making it possible for the "scaled" momentum (p/s) to cover the *infinite* range required by the canonical ensemble's distribution function,

$$f(q, p)_{\text{canonical}} \equiv e^{-q^2/2} e^{-p^2/2}/(2\pi)\ .$$

Generally Hamilton's motion equations for *any* (q, p) coordinate-momentum pair are :

$$\dot{q} = +(\partial\mathcal{H}/\partial p)\ ;\ \dot{p} = -(\partial\mathcal{H}/\partial q)\ .$$

In addition to the (q, p) pair the Nosé oscillator has also the time-scaling variable s and its conjugate momentum $p_s = \zeta$ making up a second coordinate-momentum pair (s, ζ). The motion of the Nosé oscillator in its four-dimensional phase space (q, p, s, ζ) follows from his Hamiltonian :

$$\mathcal{H}_N \longrightarrow \dot{q} = (p/s^2) \; ; \; \dot{p} = -q \; ; \; \dot{s} = \zeta \; ; \; \dot{\zeta} = (p^2/s^3) - (1/s) \, [\text{ Nosé }] \, .$$

Because the value of the Hamiltonian is constant the motion takes place in the three-dimensional volume where $\mathcal{H}_N = 0$. That volume is unbounded. So long as the *scaled* kinetic temperature is less than unity, $(p/s)^2 < 1$, *any* (q, ζ) combination is accessible by choosing a sufficiently small value of s (with an even smaller value of $p < s$) . We saw in **Figure 1** that the scale factor s ranges over more than four orders of magnitude. As a result Nosé's equations of motion present numerical challenges. Fortunately there is a way to temper the singular behavior of $\dot{\zeta}$, as was clarified by Dettmann and Morriss a dozen years after Nosé's work[6].

A.   Dettmann and Morriss' 1996 Contribution : a New Oscillator Hamiltonian

Their contribution is an alternative fully-Hamiltonian description of the *same* trajectories but with all of Nosé's rates given above multiplied by s . Here $\mathcal{H}_D$ is that Hamiltonian, followed by the new, generally slower smoother rates it generates :

$$\mathcal{H}_D = s\mathcal{H}_N = (1/2)[\, sq^2 + (p^2/s) + s\ln(s^2) + s\zeta^2 \,] \equiv 0 \longrightarrow$$

$$\dot{q} = (p/s) \; ; \; \dot{p} = -qs \; ; \; \dot{s} = \zeta s \; ; \; \dot{\zeta} = (p^2/s^2) - 1 \, [\text{ Nosé} - \text{Hoover } \#1 \,] \, .$$

Multiplying Nosé's Hamiltonian (and thus the four rates) by s when s is small tames the singular behavior of Nosé's mechanics and is equivalent to a close relative of Nosé-Hoover mechanics, "Nosé-Hoover #1". This scaled-time improvement can be simplified further to get the usual "Nosé-Hoover #2" motion equations. Just replace the scaled momentum (p/s) with p :

$$\dot{q} = p \; ; \; \dot{p} = -q - \zeta p \; ; \; \dot{s} = s\zeta \; ; \; \dot{\zeta} = p^2 - 1 \, [\text{ Nosé} - \text{Hoover } \#2 \,] \, .$$

From the numerical standpoint an advantage of this second #2 set is the *irrelevance* of the scaling variable s . The evolution of $\{ \, q, p, \zeta \, \}$, still in a three-dimensional space extending to infinity, can be determined without any consideration of s provided that H vanishes.

We urge the reader to focus on the unusual condition $\mathcal{H}_D \equiv 0$. This choice is necessary to the derivation of the [Nosé-Hoover #1] equations in the absence of time scaling. The vanishing Hamiltonian makes it possible to simplify the expression for $\dot{\zeta}$:

$$\dot{\zeta} = -(\partial \mathcal{H}_D / \partial s) = -(1/2)[\; q^2 - (p/s)^2 + \ln(s^2) + \zeta^2 + 2\;]\; \overset{\mathcal{H}_D = 0}{=} (p/s)^2 - 1 \;.$$

B.   Hoover's 1985 Contribution : Nosé-Hoover Motion equations *via* Liouville

Let us take a moment to detail Hoover's much simpler 1985 derivation of the three-equation subset of the [Nosé − Hoover #2] equations[4]. Begin with the augmented set of oscillator motion equations with a friction coefficient ζ which acts in a characteristic relaxation time τ :

$$\dot{q} = p \;;\; \dot{p} = -q - \zeta p \;;\; \dot{\zeta} = [\; (p^2/T) - 1 \;]/\tau^2 \;.$$

Here ζ is the "friction coefficient" or "control variable". If the kinetic temperature p^2 exceeds the target temperature T the friction increases, slowing p. If instead p^2 is too cool, less than T, the friction is reduced and can become negative, accelerating the oscillator. Provided only that a stationary state results, the long-time-averaged value $\langle \dot{\zeta} \rangle$ is necessarily zero so that the kinetic temperature p^2 eventually reaches its target :

$$\langle \dot{\zeta} \rangle = \langle [\; (p^2/T) - 1 \;]/\tau^2 \rangle = 0 \longrightarrow \langle p^2 \rangle = T \;.$$

A remarkable feature of the motion equations is that they leave Gibbs' canonical distribution function (or probability density) unchanged. Suppose that

$$f(q, p, \zeta, T) = (\tau/T)(2\pi)^{-3/2} e^{-q^2/2T} e^{-p^2/2T} e^{-(\zeta\tau)^2/2}$$

and consider the rate of change of probability density in $r = (q, p, \zeta)$ space as a result of the continuity equation for the flow $v = (\dot{q}, \dot{p}, \dot{\zeta})$:

$$(\partial f/\partial t) = -\nabla_r \cdot (fv) \equiv$$

$$-f[\; (\partial\dot{q}/\partial q) + (\partial\dot{p}/\partial p) + (\partial\dot{\zeta}/\partial\zeta)\;] - \dot{q}(\partial f/\partial q) - \dot{p}(\partial f/\partial p) - \dot{\zeta}(\partial f/\partial\zeta) =$$

$$-f[\; 0 - \zeta + 0 - (q/T)p - (p/T)(-q - \zeta p) - \zeta\tau^2\{\; [\; (p^2/T) - 1 \;]/\tau^2 \;\}\;] \equiv 0 \;.$$

The vanishing rate of change throughout (q, p, ζ) space implies that Gibbs' distribution is left unchanged by the flow. By design the control variable responds to $(p^2/T) - 1$ in a characteristic time τ .

Here and throughout we have consistently modified Nosé's original work[1,2], replacing his $(2/s)$ by $(1/s)$ and his p_s by ζ in order to match the alternative Nosé-Hoover description of the oscillator trajectory. The wide-ranging values of the time-scaling variable s (see again **Figure 1**) make the Nosé equations so "stiff" that an accurate fourth-order fixed-timestep Runge-Kutta solution of the equations for a typical time of 10^6 would require 10^{13} timesteps with $dt = 10^{-7}$. A few years of laptop time !

Let us summarize what we know from this Gibbsian and Hamiltonian background information in statistical mechanics and Nosé's temperature-dependent dynamics. [1] Nosé's mechanics generates stiff motion equations which are difficult to solve with conventional methods. [2] By scaling the time and redefining the momentum, $(p/s) \to p$, a more manageable set of equations consistent with Gibbs' canonical distribution results. [3] Exactly these same motion equations can be derived directly from the phase-space continuity equation if one insists that the friction coefficient ζ imposes the kinetic temperature T on the dynamics. The situation is ideal because we have several ways to check our work. Apart from the time the stiff Nosé equations and the smooth Nosé-Hoover equations have identical solutions ! Because our goal is learning to solve the stiff set :

$$\dot{q} = (p/s^2) \; ; \; \dot{p} = -q \; ; \; \dot{s} = \zeta \; ; \; \dot{\zeta} = (p^2/s^3) - (1/s) \; ,$$

we turn next to developing suitable adaptive integrators.

III. STIFF OSCILLATOR SOLUTIONS *VIA* ADAPTIVE RUNGE-KUTTA

The original work on the stiff oscillator problem[3,4] was frustrated by huge and rapid variations in p and s. Stiff equations were unusual in the molecular dynamics simulations of the 1980s. Researchers with backgrounds in simulation were not familiar with "adaptive" integrators. On the other hand researchers in control theory and heat transfer *often* used the 1969 Runge-Kutta-Fehlberg integrator to solve their own stiff equations. That Fehlberg modification of the classic Runge-Kutta methods of the early 20th century, compares fourth-order and fifth-order versions of a trajectory integration for a single step dt . The two

integrals over dt provide a criterion for increasing or decreasing dt on the next timestep. If the discrepancy is "too large" the timestep is reduced. If it is "too small" the timestep is increased. In this way the discrepancy between the two estimates can be restricted to an error band. If the discrepancy is too large an alternative to proceeding with the better RK5 estimate is to repeat the current step with smaller and smaller dt until the discrepancy falls within the acceptable band. Suitable bandwidths for double precision and quadruple precision are 10^{-12} to 10^{-10} and 10^{-24} to 10^{-20}.

Rather than comparing RK4 and RK5 one can just as well compare an iteration with dt to two successive iterations with $(dt/2)$. We have adopted that choice here. We compare two RK4 integrations $[\, dt \; versus \; (dt/2) + (dt/2) \,]$, in these demonstration problems, comparing a full timestep integration of the vector $x = (q, p, \zeta)$ or (q, p, s, ζ) from t to $t + dt$ with the result of two half-timestep integrations of the initially identical vector y :

```
call rk4(x,xp,dt/2.0d00)
call rk4(x,xp,dt/2.0d00)
call rk4(y,yp,dt/1.0d00)
errerr = (x(1)-y(1))**2 + (x(2)-y(2))**2 + (x(3)-y(3))**2 + (x(4)-y(4))**2
error = dsqrt(errerr)
if(error.gt.10.0d00**(-10)) dt = 0.5d00*dt
if(error.lt.10.0d00**(-12)) dt = 2.0d00*dt
```

The variables $(\mathtt{x,xp,y,yp})$ are vectors containing the integration variables $(\mathtt{x,y})$ and the righthand sides $(\mathtt{xp,yp})$ of the differential equations of motion. Comparing the single-timestep $\mathtt{y}$ solution to the double-timestep $\mathtt{x}$ solution provides criteria for increasing or decreasing the timestep dt. In either case the less-accurate vector, y, is set equal to the more nearly accurate vector x before the next timestep is undertaken.

As a quick demonstration problem we choose for our standard initial condition $(q, p, s, \zeta, \mathcal{H}) = 2.4, 0, e^{-2.88}, 0, 0)$ because this choice corresponds to the Dettmann Hamiltonian value for which the Nosé and Nosé-Hoover motion equations provide (apart from numerical errors) *identical* trajectories:

$$2\mathcal{H}_D = q^2 + (p/s)^2 + \ln(s^2) + \zeta^2 = 2.4^2 + 0 - 5.76 + 0 \equiv 0 \ .$$

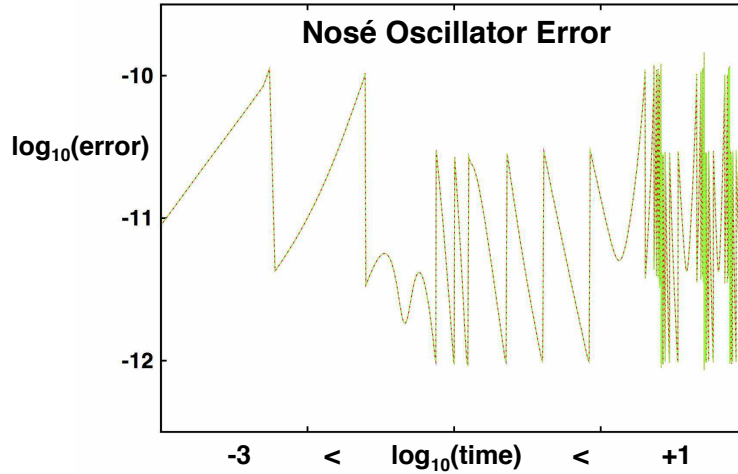**Figure 2** shows a short history of the rms discrepancy between the single and double-step

Nosé Oscillator Error

FIG. 2: Sample variation of the rms integration errors within the band from 10^{-12} to 10^{-10} with $0.001 < $ time $ < 10$. Our standard initial condition $(q, p, s, \zeta, \mathcal{H}) = (2.4, 0, e^{-2.88}, 0, 0)$, for which $\mathcal{H}$ vanishes, was used. Although both double-precision and quadruple-precision results are shown here the difference is barely visible on the scale of this plot.

versions of

$$\dot{q} = (p/s^2) \; ; \; \dot{p} = -q \; ; \; \dot{s} = \zeta \; ; \; \dot{\zeta} = (p^2/s^3) - (1/s) \; .$$

The first step is taken with $dt = 0.001$ with the calculation proceeding whenever the discrepancy [with subscripts indicating the number of steps] :

$$\sqrt{(q_1 - q_2)^2 + (p_1 - p_2)^2 + (s_1 - s_2)^2 + (\zeta_1 - \zeta_2)^2}$$

is less than 10^{-10} and otherwise proceeding with a timestep half as large. When the discrepancy falls below 10^{-12} the timestep is doubled. As a good first exercise the reader is encouraged to reproduce **Figure 2** . For the relatively short time interval in the Figure the difference between double- and quadruple-precision simulations (see below) is barely noticeable.

Any number of modifications of the algorithm can be considered and constitute useful student exercises. There is an interesting downside to existing adaptive integrators. Because the *past* is different to the *future* adaptive integrators are not reversible. This means that the

10

"accuracy" of such algorithms cannot be checked directly. One can easily check a conserved quantity, like Newtonian energy, equally well in both time directions, but trajectory accuracy requires a more elaborate investigation[12]. One criterion is the crossing of the $p = 0$ section. One should get the same number of crossings forward and backward with a good adaptive integrator.

Because atomistic mechanics problems are typically time-reversible, as are *all* the problems discussed in the present work, we thought it desirable to develop a *time-reversible* adaptive integrator. We have approached this by averaging the forward and backward errors at each point in order to define an error independent of the direction of time, using that error to decide on the magnitude of the local timestep. Although this doubles the computational time it is quite a reasonable price to pay for a robust integrator intended for demonstration problems with time-reversible dynamics. Because our approach is only approximate developing a time-reversible adaptive integrator remains a worthy research goal.

The freeware "gfortran" FORTRAN compiler from the GNU Project is routinely used in numerical work with "double precision" arithmetic (about sixteen decimal digits) through the global typing declaration for floating-point variables :

```
implicit double precision (a-h,o-z)
```

With this convention variables in the interval `i-n` are integers. For stiff problems *quadruple precision* simulations (with about thirty-four decimal digits) are useful. In gfortran this entails a minor change in the compile command :

```
gfortran -O -o xcode code.f → gfortran -O -o xcode -freal-8-real-16 code.f
```

These oscillator models have both *stable* and *unstable* "chaotic" solutions. In the latter case the effects of small changes in the initial conditions increase exponentialy in time as the solution proceeds. Choosing such a chaotic initial condition for the Nosé oscillator and an initial timestep $dt = 0.001$ generates a billion-timestep adaptive trajectory without any numerical difficulties. **Figure 3** shows the variation of the adaptive timestep on a semilogarithmic plot for a chaotic problem. As a check of such sensitive trajectories other integrators can be used and compared. Though chaos prevents our ever finding *the* solution to an initial-value dynamics problem it cannot prevent our finding a *reasonable* one !
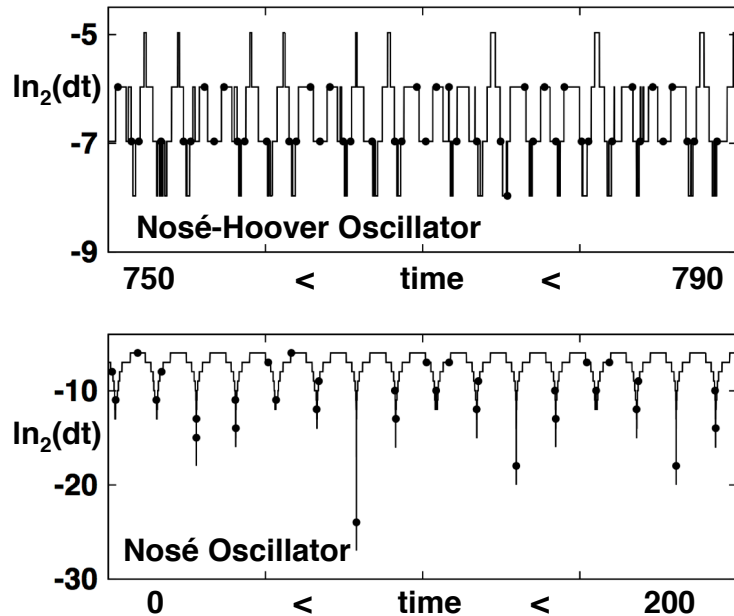
FIG. 3: Nosé and Nosé-Hoover (q, p, s, ζ) oscillator variation of $\ln_2(dt)$ with time using double-precision adaptive integration with the rms error confined between 10^{-12} and 10^{-10}. Penetrations of the $p = 0$ plane are indicated by filled circles. The Nosé data cover about 88.7 thousand timesteps while the Nosé-Hoover correspond to the range from 80.2 thousand to 84.4 thousand timesteps. In both cases the initial condition is $(q, p, s, \zeta, \mathcal{H}) = (2.4, 0, e^{-2.88}, 0, 0)$.

IV. NUMERICAL STUDIES OF THE OSCILLATOR PROBLEMS

With our computational tools well in hand, both double- and quadruple-precision, let us turn to the numerical characterization of the stiffness and chaos in the oscillator problems. These results are new and are indications of many new and promising research directions, from simple exercises to fully-fledged thesis work. To begin we quantify the Lyapunov instability of a chaotic trajectory by *measuring* the rate at which two neighboring trajectories diverge. If δ represents their separation, we characterize its single-timestep tendency toward divergence by the local Lyapunov exponent, $\lambda(t) \equiv (\dot{\delta}/\delta)$. **Figure 4** shows that the dependence of the time-averaged exponent on temperature disappears for long times. The

Nosé Oscillator with Variable Timestep

$< \lambda >$

$< \lambda^2 >$
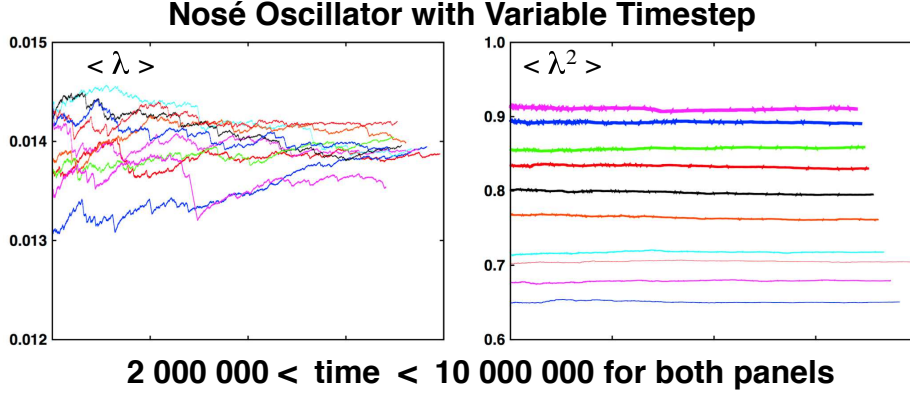
2 000 000 < time < 10 000 000 for both panels

FIG. 4: Nosé oscillator time variation of $\langle \lambda_1 \rangle$ and $\langle \lambda_1^2 \rangle$ using a reference-to-satellite offset of $\delta = 10^{-6}$ and double-precision integration. The rms error is confined within the band from 10^{-12} to 10^{-10}. As pointed out in the text the time-averaged Lyapunov exponent is temperature-independent. On the other hand the *fluctuation* of the exponent varies with temperature as shown in the right panel. The ten curves correspond to equally-spaced temperatures from 1 to 10. The time reached is a uniformly-decreasing function of temperature.

fluctuation in λ, shown to the right, has a significant dependence on temperature. Let us explain the details of such simulations.

A. Chaos and Characterization of the Nosé Oscillator's Stiffness

Nosé's oscillator problem has two kinds of solution, [1] relatively smooth and stable periodic or toroidal solutions, and [2] *unpredictable* and *chaotic* and *unstable* solutions in which nearby trajectories separate from one another exponentially fast, exhibiting "Lyapunov instability", $\delta \simeq e^{+\lambda t}$. **Figure 5** shows a cross-section of the chaotic sea. The points are plotted whenever a trajectory passes through the plane $p = 0$ or $(p/s) = 0$. They there-
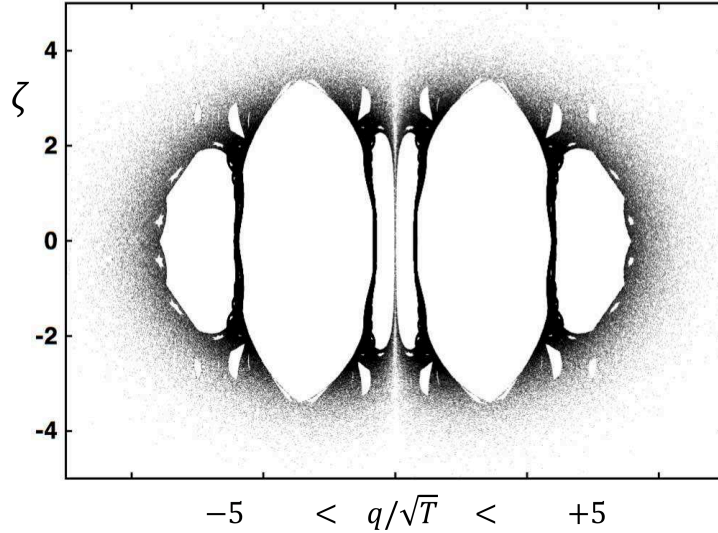
13

FIG. 5: The $(q, p, s, \zeta, \mathcal{H}) = (q, 0, s, \zeta, 0)$ cross-section of the Nosé oscillator's isoenergetic three-dimensional chaotic sea. Stable tori occupy the infinitely-many holes in the distribution. See Reference 3 for many examples. The largest Lyapunov exponent in the sea is $\lambda_1 = 0.046$ so that the chaos is relatively "weak" or "slow". *Exactly the same* cross-section results from the isothermal Nosé-Hoover oscillator equations, for which the largest Lyapunov exponent is even slower, 0.0145. Despite the similar Lyapunov exponents and identical cross sections the Nosé oscillator has huge fluctuations in its rate of phase-space exploration, and requires an adaptive integrator in order to reproduce the cross-section shown here. The abscissa reflects the scaling of the coordinate q and momentum p [(p/s) in the Nosé-Hoover case] with the square root of the temperature T . This million-point section applies to both the Nosé and Nosé-Hoover oscillator trajectories which share a common chaotic sea when $\mathcal{H}$ vanishes.

fore reflect the product of the probability density and the speed normal to the plane, $| \dot{p} |$, the "flux" :

$$| q | f(q, 0, s, \zeta) \propto | q | f(q, 0, \zeta) \propto | q | e^{-q^2/2} e^{-\zeta^2/2} .$$

The stationary distribution satisfying $(\partial f / \partial t) = 0$ is Gaussian in all three Nosé-Hoover state variables (q, p, ζ) . The cross section in **Figure 5**, and even the flux through it, are exactly the same in Nosé and Nosé-Hoover dynamics (because the trajectory is the same, with the same velocity *at* the $p = 0$ plane, independent of s) : $\dot{p}_N = \dot{p}_{NH} = -q$.
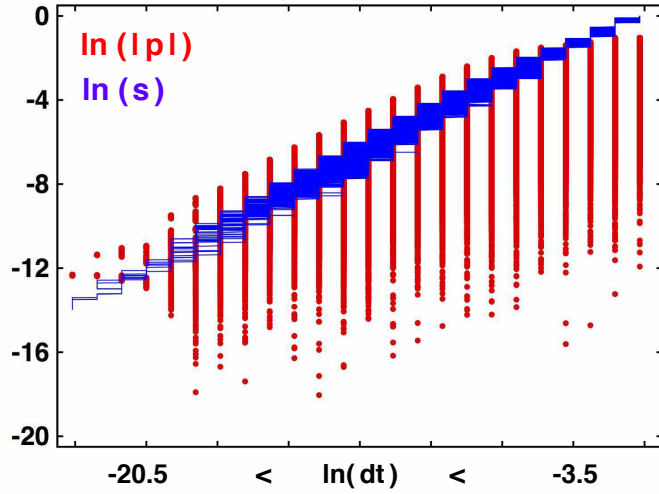
FIG. 6: Dependence of the speed $|\,p\,|$ and scale factor s on the variable timestep dt. Both variations are close to linear. The adaptive fourth-order Runge-Kutta integrator maintains a single-step rms error between the limits of 10^{-12} and 10^{-10} . The plot includes one million double-precision Nosé oscillator timesteps in the chaotic sea with $\mathcal{H} = 0$.

Let us delve into the details of the chaotic sea from the perspective of Nosé's oscillator, using what we consistently adopt as our standard chaotic initial condition :

$$(q, p, s, \zeta) = (2.4, 0, e^{-2.88}, 0) \longrightarrow \mathcal{H}_N = (1/2)[\; q^2 + (p/s)^2 + \ln(s^2) + \zeta^2\;] \equiv 0 \;.$$

One way (there is no consensus) to quantify the oscillator's "stiffness" is to record the range of the time-scaling factor s which is responsible for the stiffness. Another way is to record the range over which the timestep must be varied in order to solve the equations with a given integrator. We have used the classic fourth-order Runge-Kutta integrator, increasing or decreasing dt as needed for accuracy. All three algorithmic "variables" $(s, |\,p\,|, dt)$ show a roughly linear correlation in the log-log plot of **Figure 6**. The stiffness gives a rough correspondence between $\ln(dt)$ and $\ln(s)$. Because the scaled momentum is proportional to $\sqrt{T}$, one in the figure, $|\,p\,|$ is roughly proportional to s and to dt . To solve this same Nosé oscillator problem with a *fixed* timestep would require $dt \simeq 0.0000001$.

By way of contrast the smooth Nosé-Hoover #2 equations can be solved with the clas-

sic fourth-order Runge-Kuttta integrator for two billion double-precision timesteps (roughly 15 decimal digits) with $dt = 0.01$, reaching a time of 20,000,000 without any difficulty. The three-dimensional initial condition, $(q, p, \zeta) = (2.4, 0, 0)$, corresponds to the four-dimensional $(q, p, s, \zeta) = (2.4, 0, e^{-2.88}, 0)$ condition used in **Figure 2**. The Nosé-Hoover solution generates more than five million penetrations of the $p = 0$ cross-sectional plane. With this fixed timestep the Nosé oscillator's progress is roughly one hundred thousand times slower, while generating *exactly the same* $(q, p/s, \zeta)$ states.

B.   Chaos and the Local Lyapunov Exponent $\lambda(t)$ as a Stiffness Criterion

An alternative measure of stiffness can be based on the local (instantaneous) Lyapunov exponent. The local exponent describes the rate $\lambda(t)$ at which two nearby trajectories tend to separate, $\dot{\delta} = \lambda \delta$. Choosing a satellite trajectory x_s constrained to a distance $\delta = 0.000001$ from the reference x_r , the distance is rescaled after a time dt by multiplying the separation by a factor g (which is close to unity) :

$$x_s = x_r + g(x_s - x_r) \text{ where } g = (\ \delta/\sqrt{(x_s - x_r)^2}\ ) \simeq e^{-\lambda dt}.$$

The local Lyapunov exponent is $\lambda(t) = -\ln(g)/dt$. **Figure 7** shows two sections of a typical time history of λ from an adaptive solution of Nosé dynamics. The central Nosé peak at a time of 5.0862 was resolved by an adaptive integrator which chose a timestep of 2×10^{-9} for the peak shown. The corresponding time for Nosé-Hoover #2 dynamics is 16.42, and corresponds to a broad minimum in s. The amplitudes and the required numbers of timesteps differ by about six orders of magnitude for the two equivalent representations of a thermostated oscillator trajectory.

Nosé got around the stiffness of his motion equations by arbitrarily multiplying the right-hand sides of each of his four Hamiltonian equations of motion by s. This trick doesn't change the four-dimensional trajectory at all if we visualize the trajectory as a one-dimensional path in four-dimensional (q, p, s, ζ) space. But the *rate* at which the path is followed is changed by the factor s. Nosé termed this change of rate "scaling the time" and uses it in his 1984 papers. His "real" *versus* "virtual" variables helped to make his work relatively difficult to fathom. Now that we have been able to solve his equations directly, with adaptive integrators we have attained a good picture of the Lyapunov instability and stiffness of the original
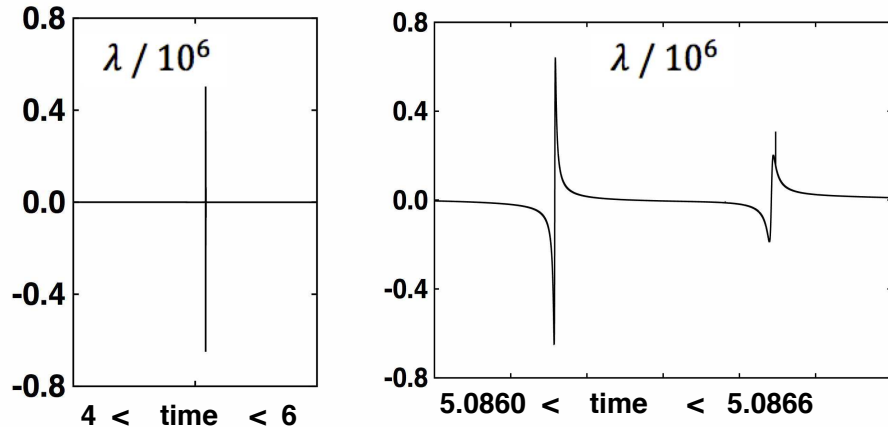
FIG. 7: Nosé oscillator local Lyapunov exponent in the chaotic sea as a function of time with $\delta = 10^{-6}$ and the quadruple-precision error confined to the band between 10^{-28} and 10^{-24}. The left panel shows data with timesteps from 1.63 to 3.07 million. The right panel includes data between 2.01 and 2.16 million timesteps. The standard chaotic initial condition $(q, p, s, \zeta, \mathcal{H}) = (2.4, 0, e^{-2.88}, 0, 0)$.

Nosé equations. Let us summarize the present situation.

V. SUMMARY AND OUTLOOK

A. Adaptive Integrators and the Use of Mappings

Today's "realistic" computer models, typically representing thermostated aqueous solutions, involve a host of practical computational issues.[13] One we did not detail here is the need for integration techniques dealing with discontinuous righthand sides. Adaptive integrators are often used in artificial demonstration problems with *singular* righthand sides.
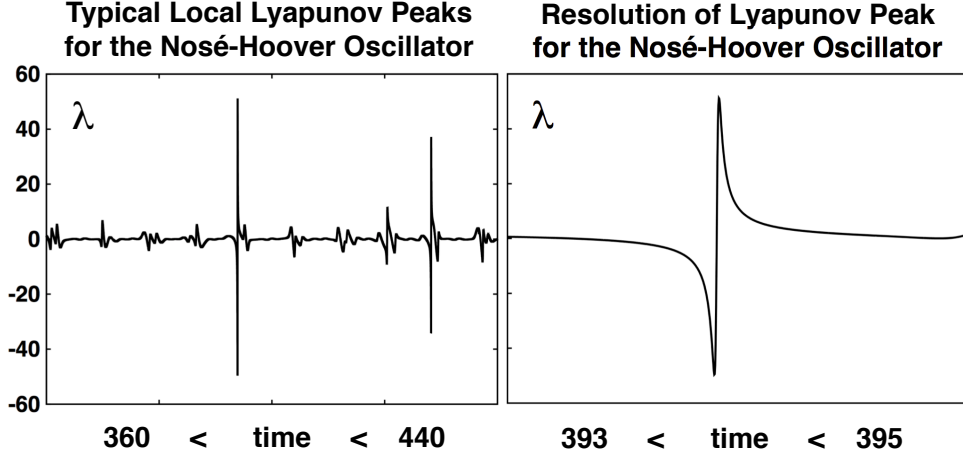
17

Typical Local Lyapunov Peaks for the Nosé-Hoover Oscillator

Resolution of Lyapunov Peak for the Nosé-Hoover Oscillator

FIG. 8: Nosé-Hoover (q, p, s, ζ) local Lyapunov exponent variation in the chaotic sea with a closeup showing the resolution of a typical "large" peak. The maximum time shown, 440, corresponds to a total of 286 575 timesteps with dt confined to the interval 10^{-16} to 10^{-14} using double-precision arithmetic. The satellite-to-reference separation is $\delta = 10^{-6}$.

Discontinuous jumps of a control variable ["Bang-Bang Control"] is an example.

Special precautions need to be taken when the dynamics itself is singular (as in hard-sphere or square-well dynamics), replacing the smooth separation rate $\lambda(t)$ with a singular map^{14} as the collisional "events" occur. Although this has been the typical approach in molecular dynamics simulations since the 1980s, the mapping technique is unfamiliar to most workers in dynamical systems simulations. In hard-sphere molecular dynamics, going back to Alder and Wainwright's pioneering work of the middle 1950s[15], with thousands or millions of degrees of freedom, it is usual to integrate up to the moment of the next collision, change the momenta of the colliding particles *at* the collision, and then continue on until the next collision. These "event-driven" simulations are another example of the need for two or

more solution strategies for the underlying differential equations.

B.   Characterizing Chaos with Lyapunov Instability

Where chaos is concerned, which is typical of "interesting" problems, Lyapunov instability is most easily quantified by following two neighboring trajectories. The relative motion of the two trajectories can be constrained by using a Lagrange multiplier. Alternatively the distance between the two trajectories can be rescaled. Either way the original separation length is recovered at the end of each timestep. The logarithm of the scale factor required to do this is simply related to the local Lyapunov exponent. These two approaches provide the largest Lyapunov exponent λ_1 , the mean separation rate over a long simulation, $\dot{\delta} = \lambda_1 \delta$. The Lagrange multiplier approach can also be applied to a linearized version of the equations at the expense of additional algebra. All three of these techniques are useful tools which can benefit from adaptive integration[16].

Chaotic systems will always be a challenge. Joseph Ford[17] emphasized that numerical methods are unable to follow any chaotic trajectory accurately for very long. The only convincing test of accuracy is the reproducibility of the trajectory itself. Simple reversal of a trajectory or conservation of energy are not reliable criteria for accuracy[15]. Numerical chaotic trajectories can simulate these difficult situations and do provide "weak" averages which are accurate despite the lack of global accuracy in the computed trajectory. This good fortune is likewise typical of event-driven dynamical systems. It is evident that *no* numerical methods are capable of precise solutions of such problems. Adaptive integrators are a useful tool for producing "reasonable" chaotic trajectories, inaccurate though they may be.

C.   Unique Features of the Nosé-Based Oscillator Models

Because all three oscillator models, [Nosé, Nosé-Hoover #1, and Nosé-Hoover #2, or N and NH] share common trajectories, their travel times and their Lyapunov exponents are related in an intriguing way, unique in our dynamical-systems experience. At unit temperature the three models are precisely related: $\lambda_N = 3.26\lambda_{NH}$ and $\vec{t}_{NH} = 3.26\vec{t}_N$. Here the $\{\ \vec{t}\ \}$ denote travel times along a sufficiently long trajectory. The Nosé trajectory is the fastest of the three. The disparities are the result of the slower rates (by a common
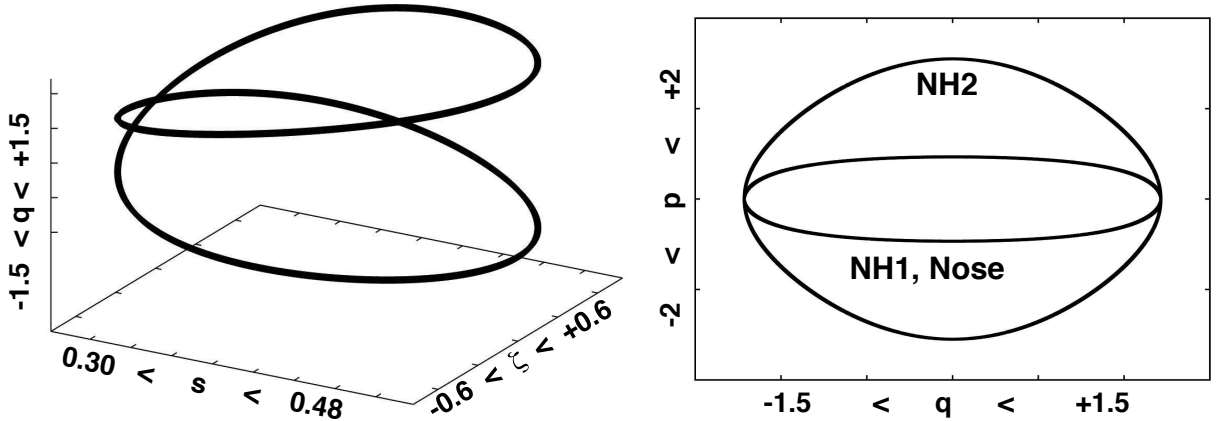
FIG. 9: At the left the vertical coordinate is q, plotted as a function of s, which is always positive, and ζ . At the right the smaller ellipse corresponds to to both the Nosé and Nosé-Hoover #1 equations. The outer ellipse represents Nosé-Hoover #2. The two Nosé-Hoover curves have a period of 5.578 while the Nosé period is "faster" 2.1655 .

factor $s < 1$) in the two versions of Nosé-Hoover dynamics. The travel times for a long trajectory in (q, p, s, ζ) space are necessarily related by the same ratio, with $\vec{t}_{NH} = 3.26\vec{t}_N$. The longtime averaged growth rate of the slower Nosé-Hoover trajectories leads to a smaller common Lyapunov exponent $\lambda_{NH\#1} = \lambda_{NH\#2} = \lambda_N/3.26$. This relationship between the time-averaged exponents does *not* hold for the local exponents, $\lambda_{NH}(t)$ and $\lambda_N(t)$.

Why not? It is evident that both dynamics share the *same* reference trajectory. It might then appear that the neighboring satellite trajectory determining $\lambda(t)$ would be the same for

20

both dynamics too. But because the local exponent responds to the time-rate-of-change of the scale factor $s(t)$ there is no simple relationship linking the local exponents. Nevertheless the relation between the rates, $(d/dt)_{NH} \equiv s(d/dt)_N$, is valid for any (q, p, s, ζ) trajectory segment with a vanishing Hamiltonian. The relation linking all the rates leads directly to the useful relations :

$$\vec{t}_{NH} = \langle\, 1/s \,\rangle_N \vec{t}_N \; ; \; \vec{t}_N = \langle\, s \,\rangle_{NH} \vec{t}_{NH} \, .$$

As an example, illustrated in **Figure 9**, consider the simplest stable periodic orbit, with initial values $(q, p, s, \zeta, \mathcal{H}) = (1.2145, 0.0, e^{-q^2/2}, 0, 0)$, traced out in times of $\vec{t}_{NH} = 5.5781$ and $\vec{t}_N = 2.1655$. The ratios of the two times are related to the mean values of $s^{\pm 1}$ averaged over the orbit :

$$\vec{t}_{NH}/\vec{t}_N = 5.5781/2.1655 = 2.5759 = \langle\, s^{-1} \,\rangle_N \; ;$$

$$\vec{t}_N/\vec{t}_{NH} = 2.1655/5.5781 = 0.3882 = \langle\, s^{+1} \,\rangle_{NH} \, .$$

An interesting feature of the oscillator problems is that *the largest Lyapunov exponent is independent of temperature.* See the lefthand side of **Figure 4**. The righthand side *does* show temperature dependence. The *fluctuation* of the exponents (hardly distinguishable from $\langle\, \lambda_1^2(t) \,\rangle$) increases with temperature for temperatures greater than 2.

We can *prove* the temperature independence shown in **Figure 4**. If we consider the *temperature-dependent* Nosé-Hoover #2 equations and introduce new variables,

$$Q \equiv (q/\sqrt{T}) \; ; \; P \equiv (p/\sqrt{T}) \; ; \; Z = \zeta \, ,$$

the temperature-independent result shows that the largest Lyapunov exponent (but not its fluctuation) is indeed temperature independent (This is because a *linear* change of scale leaves the time-averaged *logarithmic* growth rate unchanged) :

$$\dot{q} = p \to \dot{Q} = P \; ; \; \dot{p} = -q - \zeta p \to \dot{P} = -Q - ZP \; ; \; \dot{\zeta} = (p^2/T) - 1 \to \dot{Z} = P^2 - 1 \, .$$

In Section IIB we saw that the temperature-dependent (q, p, ζ, T) Nosé-Hoover equations provide a stationary solution from Liouville's Theorem :

$$f \propto e^{-q^2/2T} e^{-p^2/2T} e^{-\zeta^2 \tau^2/2} \to$$

$$\dot{q} = p \; ; \; \dot{p} = -q - \zeta p \; ; \; \dot{\zeta} = [\, (p^2/T) - 1 \,]/\tau^2 \, ,$$

Just as in the simpler case with T and τ equal to unity we can find a corresponding $\mathcal{H}_D$:

$$2\mathcal{H}_D = sq^2 + (p^2/s) + Ts\ln(s^2) + (s\zeta^2/T\tau^2) \equiv 0 .$$

We remarked on the disparity of the Nosé and Nosé-Hoover Lyapunov exponents. The Nosé oscillator exponent is 0.046 ± 0.001 while the two Nosé-Hoover exponents are smaller, $0.014_5 \pm 0.0001$. **Figure 7** illustrated, on two very different scales, a typical excursion of the local Lyapunov exponent in Nosé's stiff case. On the scale of the figure at the left the variation looks *singular*, but it is actually *smooth* when adaptive integration is used to control the scale of the smallest timestep, which is 10^{-9} . **Figure 8** shows similar data for the Nosé-Hoover version of the same problem. In that case no special precautions need be taken. A fixed timestep of 0.001 is perfectly adequate for accurate estimates of the local Lyapunov exponent.

D.   Challenges and Ideas for Future Work

In bringing this discussion of adaptive integrators to a close let us mention that there is a significant variation in the *topology of* the chaotic and regular solutions for our oscillator models where the thermostating is "fast" :

$$\dot{\zeta} = [\, p^2 - 1\,] \longrightarrow \dot{\zeta} = [\, p^2 - 1\,]/\tau^2$$

[when the response time τ is small]. In particular, fast thermostating generates infinite numbers of intricately *knotted trajectories*, many of which are described in References 18 and 19 . These simple oscillator models, with quadratic ordinary differential equations (and their nonequilibrium fractal relatives, where temperature is a function of the coordinates), can generate *interlinked rings* in phase space. An example is described in our own very recent work with Puneet Patra[20]. These models' chaotic trajectories, with their knots, and interlinked rings could easily fill an entertaining and profusely-illustrated Book on the subject. We urge the reader to explore and enjoy these topics. In this spirit we append here three colored Nosé $p = 0$ sections illustrating the dependence of $\lambda(t)$, dt, and s on (q, ζ) .

---
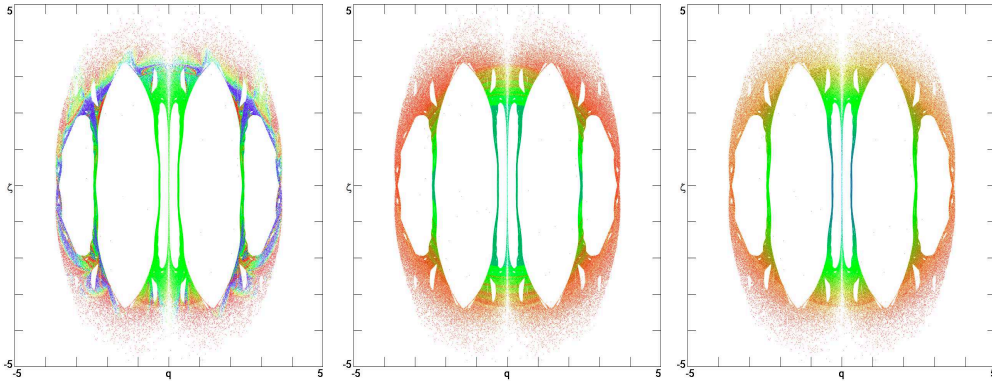
[1] S. Nosé, "A Unified Formulation of the Constant Temperature Molecular Dynamics Methods", The Journal of Chemical Physics **81**, 511-519 (1984).

[2] S. Nosé, "A Molecular Dynamics Method for Simulations in the Canonical Ensemble", Molecular Physics **52**, 255-268 (1984).

[3] H. A. Posch, W. G. Hoover, and F. J. Vesely, "Canonical Dynamics of the Nosé Oscillator: Stability, Order, and Chaos", Physical Review A **33**, 4253-4265 (1986).

[4] W. G. Hoover, "Canonical Dynamics: Equilibrium Phase-Space Distributions" Physical Review A **31**, 1695-1697 (1995).

[5] Wm. G. Hoover, "Mécanique de Nonéquilibre à la Californienne", Physica A **240**, 1-11 (1997).

[6] C. P. Dettmann and G. P. Morriss, "Hamiltonian Reformulation and Pairing of Lyapunov Exponents for Nosé-Hoover Dynamics", Physical Review E **55**, 3693-3696 (1997).

[7] W. G. Hoover and B. L. Holian, "Kinetic Moments Method for the Canonical Ensemble Distribution", Physics Letters A **211**, 253-257 (1996).

[8] D. Kusnezov, A. Bulgac, and W. Bauer, "Canonical Ensembles from Chaos", Annals of Physics **204**, 155-185 (1990).

[9] W. G. Hoover, J. C. Sprott, and P. K. Patra, "Ergodic Time-Reversible Chaos for Gibbs' Canonical Oscillator", Physics Letters A **379**, 2935-2940 (2015) = arχiv: 1503.06749.

[10] P. K. Patra and B. Bhattacharya, "A Deterministic Thermostat for Controlling Temperature Using All Degrees of Freedom", The Journal of Chemical Physics **140**, 064106 (2014).

[11] J. C. Sprott, *Chaos and Time-Series Analysis* (Oxford University Press, Oxford, 2003) page 67.

[12] Wm. G. Hoover and C. G. Hoover, "Comparison of Very Smooth Cell-Model Trajectories Using Five Symplectic and Two Runge-Kutta Integrators", Computational Methods in Science and Technology **12**, 109-116 (2015).

[13] R. L. Davidchack, "Discretization Errors in Molecular Dynamics Simulations with Deterministic and Stochastic Thermostats" = arχiv:1412.7067.

[14] Ch. Dellago and H. A. Posch, "Lyapunov Exponents of Systems with Elastic Hard Collisions", Physical Review E **52**, 2401-2406 (1995).

[15] B. J. Alder and T. E. Wainwright, "Molecular Motions", Scientific American **201**, 113-126 (1959).

[16] W. G Hoover and C. G. Hoover, *Simulation and Control of Chaotic Nonequilibrium Systems* (World Scientific Publishers, Singapore, 2016).

[17] T. Uzer, B. Chirikov, F. Vivaldi, and G. Casati, "Joseph Ford", Physics Today **48**, 88 (1995).

[18] L. Wang and X-S. Yang, "The Invariant Tori of Knot Type and the Interlinked Invariant Tori in the Nosé-Hoover System", The European Physics Journal B **88**, 78-82 (2015) = arχiv : 1501.03375 .

[19] L. Wang and X-S. Yang, "A Vast Amount of Invariant Tori in the Nosé-Hoover Oscillator", Chaos **25**, 123110 (2015).

[20] P. K. Patra, W. G. Hoover, C. G. Hoover, and J. C. Sprott, "The Equivalence of Dissipation from Gibbs' Entropy Production with Phase-Volume Loss in Ergodic Heat-Conducting Oscillators", International Journal of Bifurcation and Chaos (in press, 2016) = arχiv : 1511.03201 (2015).